



Design and fabrication of size-controlled Pt–Au bimetallic alloy nanostructure in carbon nanofibers: a bifunctional material for biosensors and the hydrogen evolution reaction

Bin Zhang¹, Han Zhu¹, MeiLing Zou², XinRong Liu¹, Hui Yang¹, Ming Zhang¹, WeiWei Wu¹, JuMing Yao¹, and MingLiang Du^{1,*}

¹Department of Materials Engineering, College of Materials and Textiles, Zhejiang Sci-Tech University, Hangzhou 310018, People's Republic of China

²Zhejiang Institute of Medical device testing, Hangzhou 310018, People's Republic of China

Received: 12 October 2016

Accepted: 20 March 2017

Published online:

28 March 2017

© Springer Science+Business Media New York 2017

ABSTRACT

Small-sized and well-dispersed Pt–Au nanoparticles (Pt–AuNPs) grown on carbon nanofibers (Pt–AuNPs/CNFs) with excellent electroanalytical and electrocatalytic performance in the detection of H₂O₂ and the catalytic hydrogen evolution reaction (HER) were designed and fabricated via electrospinning technology and an in situ thermal reduction process. Large numbers of Pt–AuNPs were homogeneously distributed on the CNFs. A Pt–AuNP/CNF hybrid with low Pt content was utilized as a bifunctional electrocatalyst, exhibiting a higher response current of 116 μA without an enzyme in the detection of H₂O₂ and a lower overpotential ($j = 10 \text{ mA cm}^{-2}$ at -235 mV) and Tafel slope ($84 \text{ mV decade}^{-1}$) for HER than the PtNPs/CNFs and the AuNPs/CNFs. These results were ascribed to the specific nanostructure of the well-dispersed Pt–AuNPs, the favorable electron transport capability, the excellent durability of the CNFs, and the enhanced surface-specific area of the Pt–AuNPs/CNFs. This study offers a green and facile method for constructing a specific bimetallic nanostructure for application in catalytic fields.

Introduction

Recently, bimetallic nanomaterials existing as homogeneous alloys or heterogeneous core shell structures have received increasing attention [1–5] because of their superior catalytic performance, enhanced

electron transport rate, and greater selectivity and durability compared to their monometallic counterparts [6–8]. In particular for bimetallic nanoparticles (NPs), the interaction effects are usually synergic effects rather than as a simple combination of the properties of two monometallic NPs [1, 9].

Address correspondence to E-mail: du@zstu.edu.cn

Consequently, bimetallic nanomaterials have exhibited many unique properties and have been employed in various fields [10–17]. As is well known, noble metal NPs, such as Pt and Au, exhibit extraordinary electrocatalytic and electroanalytic properties. Pt has usually acted as a benchmark for the evaluation of electrocatalysts because it possesses the most effective catalytic performance, especially for the hydrogen evolution reaction [18, 19]. Because of its unique analytic ability for different reactions, Au has attracted much attention as a transition metal with low electronegativity [1]. Therefore, it is expected that the combination of the effective catalytic activity of Pt and the sensitive analytic activity of Au may generate multiple excellent properties at the same time, which has inspired many related investigations in catalytic and analytic fields [7, 20–25].

However, it is extremely difficult to fabricate a Pt–Au alloy because of the weak miscibility and facile aggregation of these elements [26–28]. At present, a variety of approaches are employed to synthesize Pt–Au alloys with different structures, such as nanoporous structures [20, 21], nanoframes [22], nanowires [29], nanocables [30], nanorods [31] and nanocages [32]. Among these approaches, Pt–AuNPs have become a hot research topic because of their large surface area, abundance of active sites and facile synthesis methods. Zhang et al. [24] applied a polyelectrolyte-assisted process to prepare Pt–AuNPs on graphene with a uniform dispersion, and the nanostructure exhibited high electrocatalytic activity and stability for formic acid oxidation. Takahashi et al. [25] synthesized Pt–AuNPs by arc-plasma deposition, and they exhibited excellent oxygen reduction reaction performance and enhanced durability. Because of their outstanding multifunctional properties in electrochemical applications, Pt–AuNPs have potential for use in bifunctional materials for different electrochemical reactions.

To date, it is still necessary and desirable to search for a suitable support for the Pt–AuNPs to enhance electrocatalytic activity. Herein, the particle size, the morphology, the nanostructure, and the dispersion of Pt–AuNPs on substrates play important roles in improving electrocatalytic performance. Carbon-based nanomaterials are usually excellent supports for the loading of nanocrystals because of their attractive conductivities, low cost, large specific surface area, abundant active sites, and fast mass transfer and charge transfer rates. Recently, large amounts

of carbonaceous materials, such as graphene [33–36], carbon nanotubes (CNTs) [37–39], carbon paper [40–42], and carbon black [43–45], have been widely applied to support the nanocrystals. Electrospun carbon nanofibers (CNFs) are an excellent carbon-based nanomaterial with a high length-to-diameter ratio and additional active sites for nanoparticle loading or deposition. In addition, CNFs exhibit higher chemical inertness, larger effective diffusion coefficient, lower cost and easier preparation over CNTs as a support material for heterogeneous catalysts. Based on our previous works, size-controlled nanocrystals loaded on CNFs were successfully constructed and fabricated via electrospinning technology and thermal reduction [46, 47]. Automatically, the synthesized nanocrystals/CNFs were utilized for electroanalysis and electrocatalysis, and the related electrochemical sensors and devices exhibited excellent performance [48, 49].

In the present investigation, we proposed a novel and facile strategy for the design and fabrication of small-sized and well-dispersed Pt–AuNPs grown on CNFs. In detail, the Pt–AuNPs/CNFs were synthesized via electrospinning technology and an in situ thermal reduction process. The Pt–AuNPs/CNFs with low Pt content were utilized as a bifunctional material for biosensors and the hydrogen evolution reaction, exhibiting a higher response current of 116 μA without enzymes in the detection of H_2O_2 and a lower overpotential and Tafel slope for hydrogen evolution reaction (HER). This study may offer a green and facile method for constructing specific bimetallic nanostructures for application in catalytic fields.

Experimental section

Materials

Chloroplatinic acid ($\text{H}_2\text{PtCl}_6 \cdot 6\text{H}_2\text{O}$, 99.9%), chloroauric acid ($\text{HAuCl}_4 \cdot 4\text{H}_2\text{O}$, 99.9%), and sulfuric acid were acquired from Shanghai Civi Chemical Technology Co., Ltd. *N,N'*-dimethylformamide (DMF) was purchased from Shanghai Shenbo Chemical Co., Ltd (China). Phosphate buffer saline (PBS), hydroquinone, and hydrogen peroxide (H_2O_2 , 30 wt%) were obtained from Hangzhou Gaojing Fine Chemical Co. Ltd. Polyacrylonitrile (PAN, $M_w \approx 1.4 \times 10^5$, copolymerized with 10 wt% methyl

acrylate) was purchased from Sinopec Shanghai Petrochemical Co., Ltd. A Nafion aqueous solution (5 wt%) was obtained from Aldrich Chemistry Co., Ltd, and other reagents were purchased from Aladdin Sinopharm Chemical Reagent Co., Ltd. (Shanghai, China). All the chemicals were used as received without further purification. Deionized water was used for all solution preparations.

Preparation of Pt–AuNPs in polyacrylonitrile (PAN) electrospun precursor solution and Pt–AuNPs embedded in polyacrylonitrile nanofibers (Pt–AuNPs/PAN)

To prepare the precursor solution, 1.5 g of PAN was first dissolved in 11 mL of DMF under moderate stirring for 2 h to obtain a homogeneous solution. Then, the mixtures were poured into a 25 mL Erlenmeyer flask (fitted with a magnet) and heated to 80 °C, with vigorous stirring by magnetic force. After 30 min, 0.05 g of chloroplatinic acid was slowly added into the Erlenmeyer flask, and the magnetic stirring was maintained until the solution was well mixed. Then, 0.075 g chloroauric acid was added into the mixture under the same conditions. With vigorous stirring for 4 h, the mixture was completely uniform, and the electrospun precursor solution was obtained. The mass ratio of Pt: Au is 2:3. The electrospun precursor solutions of PtNPs and AuNPs in PAN are similar to this procedure.

The procedure for the electrospun precursor solution was the same as that for the PAN nanofibers. The electrospun parameters: feed rate, voltage, and distance were 0.6 mL h⁻¹, 18 Kv, and 12 cm, respectively. All experiments were performed at room temperature. The electrospun nanofibrous mats were collected onto a tin foil, dried for 1 h, and then preserved in the drying oven for further use.

Synthesis of size-controlled Pt–AuNPs/CNFs

The Pt–AuNPs/CNFs were synthesized by a carbonization process. First, a piece of an electrospun nanofibrous mat (8 mm × 10 mm) was put into a homemade chemical vapor deposition tube furnace. Then, it was heated to 280 °C with a heating rate of 5 °C min⁻¹ and held for 2 h in air. In the next stage, the samples were heated to 1000 °C for graphitization

in an Ar (150 sccm) atmosphere, with a heating rate of 5 °C min⁻¹. Finally, the samples were held at the graphitization temperature for 4 h and subsequently programmed cooled to room temperature. The final Pt and Au contents of the sample were 3.09 and 5.89 wt%.

Fabrication of Pt–AuNPs/CNFs modified GCE (Pt–AuNPs/CNFs/GCE)

For the pretreatment of the bare GCE, generally, the bare GCE was ultrasonically processed in ethanol for 30 min to remove the surface residue and then polished carefully to a mirror finish with alumina slurry (diameters of 0.3 and 0.05 μm). This was followed by ultrasonic rinsing in ethanol and doubly distilled water and drying. Then, 3 mg of sample was ultrasonically dispersed in 1 mL of a mixed solvent [composed of 3:1 (v/v), isopropanol/distilled water and 30 μL of Nafion (5 wt%)], to obtain a homogeneous ink. Finally, 5 μL of ink was carefully transferred onto the GCE and dried at room temperature for a night. The modified electrodes were prepared and are denoted as Pt–AuNPs/CNFs/GCE. After solvent evaporation, the electrodes were moved to a vacuum drying oven and dried for 30 min before further characterization.

Instruments

The morphologies of the electrospun Pt–AuNPs/CNFs, PtNPs/CNFs, and AuNPs/CNFs hybrids were observed by using a JSM-6700F field-emission scanning electron microscope (FE-SEM, JEOL, Japan) at an acceleration voltage of 3 kV. Transmission electron microscopy (TEM) images were obtained by using a JSM-2100 transmission electron microscope (JEOL, Japan) at an acceleration voltage of 200 kV. The X-ray photoelectron spectra of all of the samples were recorded using an X-ray photoelectron spectrometer (Kratos Axis Ultra DLD) with an aluminum (mono) K_α source (1486.6 eV). The aluminum K_α source was operated at 15 kV and 10 mA. The B.E. resolution of the instrument was under 0.5 eV. The X-ray diffraction (XRD) patterns of the samples were analyzed by a Bruker AXS D8 DISCOVER X-ray diffractometer with Cu K_α radiation (λ = 1.5406 Å) at a scanning rate of 0.02° 2θ s⁻¹ in the 2θ range of 10–80°. All of the cyclic electrochemical measurements [cyclic voltammetry and line stripping

voltammetry (LSV)] were carried out using a CHI660E computer-controlled potentiostat (ChenHua Instruments Co., Shanghai, China) and performed in a conventional three-electrode cell with either a bare or a modified glassy carbon electrode (GCE, 3 mm in diameter) as the working electrode, a platinum electrode as the counter electrode, and a saturated calomel electrode (SCE, ChenHua Instruments Co., Shanghai, China) as the reference electrode.

Characterization of electroanalytic and electrocatalytic performance

All electrochemical experiments were performed using a CHI660E electrochemical workstation. The electrochemical measurements were taken with a typical three-electrode cell: the modified GCE (Pt–AuNPs/CNFs/GCE) as the working electrode, a platinum electrode as the auxiliary electrode, and a SCE as the reference electrode. For the electroanalytic performance, the detection of H_2O_2 was carried out in 0.1 M PBS by cyclic voltammetry at a different scan rate. In addition, a pretreatment of bubbling with high-purity nitrogen in the solution for at least 30 min was performed to remove the effect of dissolved oxygen before CV.

To assess electrocatalytic performance, the solution was first purged with high-purity nitrogen for at least 30-min prior to each experiment to protect the solution from oxygen. Then, the modified GCE was immersed into an aqueous solution of 0.5 M H_2SO_4 for cyclic voltammetry (CV) measurement at a scan rate of 50 mV s^{-1} . After that, the modified GCE was characterized by HER measurements, and the LSV was obtained at a scan rate of 2 mV s^{-1} . Meanwhile, the polarization curves were obtained after iR-compensation. Moreover, other external conditions were controlled to ensure the comparability of each experiment, and all measurements were taken at room temperature.

Results and discussion

The morphology of the as-prepared bimetallic Pt–AuNP/CNF nanostructure

Based on our previous work, the well-distributed Pt–AuNPs/PAN nanofibers were obtained through a traditional in situ reduction and electrospinning

procedure. Following the carbonization process, the embedded Pt–AuNPs underwent migration to the surface of the carbon nanofibers to form the bimetallic nanostructure [47]. Figure 1a, b, c shows the FE-SEM images of the as-prepared Pt–AuNPs/CNFs, PtNPs/CNFs, and AuNPs/CNFs, and the diameters of the nanofibers were approximately 350 ± 24 , 225 ± 18 , and 263 ± 20 nm, respectively. The three different nanoparticles were all loaded onto the surface of the CNFs homogeneously. The detailed microstructure of the synthesized metal NPs/CNFs is shown in Fig. 1d, e, f. The insets shown in Fig. 1d, e, f are the TEM images of individual carbon nanofiber, which confirmed the well-distributed nanoparticles loaded on the nanofibers. The homogeneous nanoparticles shown in Fig. 1d, e, f further confirmed the specific size-controlled nanostructure of the NPs/CNFs. Typical HRTEM images are shown in Fig. 1g, h, i, indicating their respective lattice fringes, and the insets are the sources of the HRTEM images. The blue arrows are the layer of graphite, which coated the surface of the nanoparticles and improved the stability. The lattice fringe spacing of the Pt–AuNPs/CNFs was approximately 0.196 and 0.212 nm, corresponding to the (111) and (120) planes. In addition, the lattice fringe spacing of PtNPs/CNFs and AuNPs/CNFs was 0.138 and 0.152 nm, respectively, corresponding to the (111) plane of the face-centered (fcc) crystal. Moreover, the diameter of the Pt–AuNPs, PtNPs, and AuNPs were all between 5 and 15 nm according to the FE-SEM and TEM images. The small size and uniform distribution of the NPs are expected to significantly improve electroanalytic and electrocatalytic performance.

To further verify the polycrystalline structure and detailed composition of the as-prepared Pt–AuNPs/CNFs, the HAADF-STEM, and STEM-EDS mapping images are shown in Fig. 2a. The red shaded part in Fig. 2a is the mapping region of the Pt–AuNPs/CNFs. The one-to-one display areas of Pt and Au elements in Fig. 2a indicate that homogeneous phase structure of the Pt–AuNPs/CNFs. Moreover, as shown in Fig. 2c, the EDX spectrum of the Pt–AuNPs/CNFs revealed C, N, O, Pt, and Au elements, indicating the existence of Pt–AuNPs. Figure 2d shows the line-scanned EDX spectrum, and the red line in Fig. 2b is the line-scan region, which testifies to the presence of the Pt–AuNPs/CNFs. Furthermore, the good match between the emerging positions of Pt and Au elements further confirms the

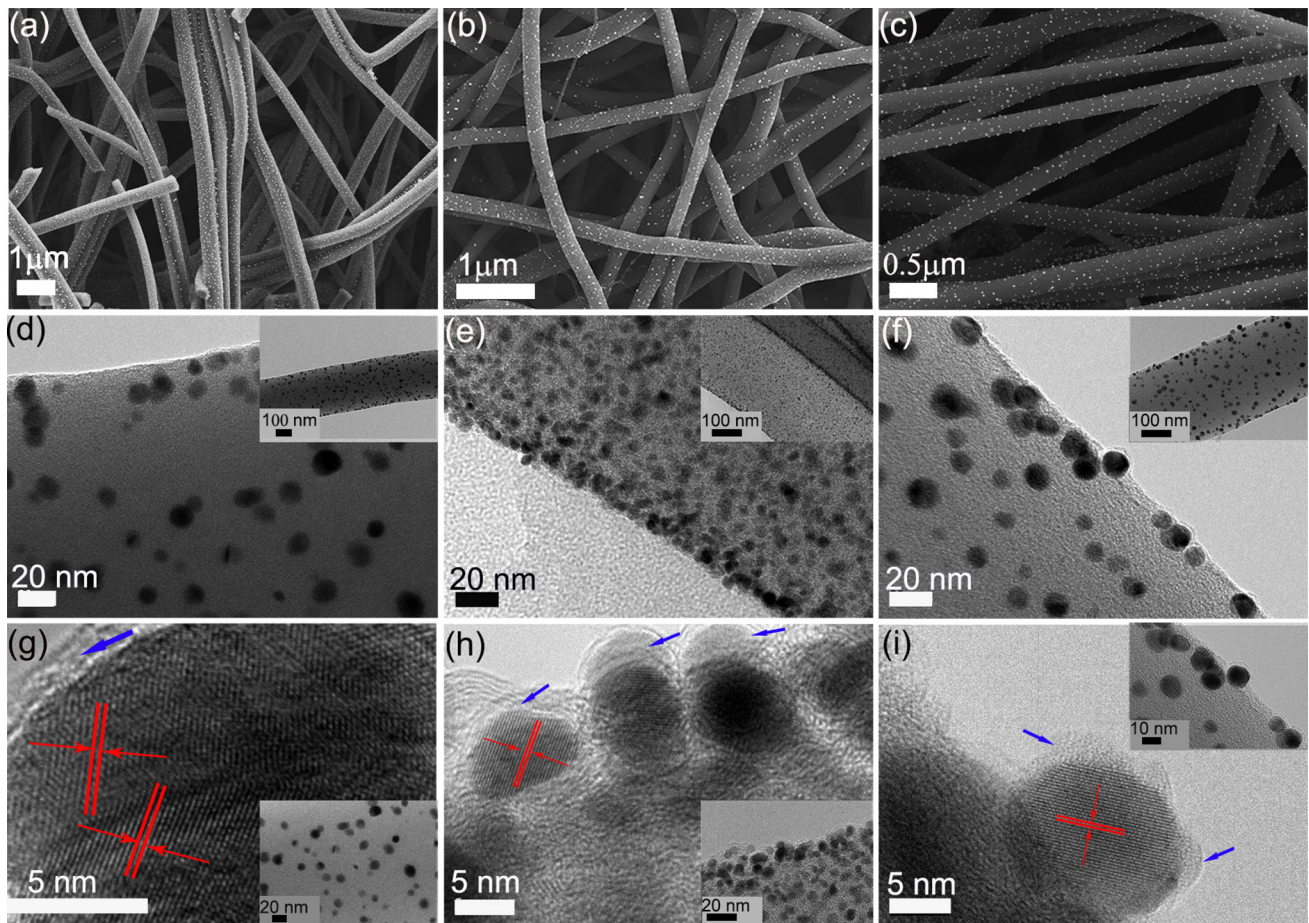


Figure 1 a–c FE-SEM images of the as-prepared Pt–AuNPs/CNFs, PtNPs/CNFs, and AuNPs/CNFs. The corresponding TEM images (d–f) and the corresponding insets are the TEM images of

single CNFs; HRTEM image (g–i) and the corresponding insets are the selected areas.

homogeneous phase structure of the Pt–AuNPs/CNFs.

Two diffraction peaks emerged in the XRD patterns of the Pt–AuNPs/CNFs and the PtNPs/CNFs and are shown in Fig. 3. The red line in the XRD pattern is the diffraction peak of the as-prepared PtNPs/CNFs, and the clear diffraction peaks are almost undetectable because of the small size of the PtNPs. However, the Pt–AuNPs/CNFs exhibit apparent diffraction peaks, suggesting the favorable crystallization of the Pt–AuNPs/CNFs. The strong and sharp diffraction peaks that appeared at 38.3° , 44.5° , 64.8° , 77.7° , and 81.8° in the Pt–AuNPs/CNFs are consistent with the (111), (200), (220), (311), and (222) planes of the Au crystal, respectively. Compared with Au JCPDS cards 04-0784, the representative diffraction peaks of Au generated a slight blue shift. Meanwhile, the diffraction peaks that appeared at 40.2° , 46.7° , and 67.9° in the Pt–AuNPs/CNFs are

in accordance with the (111), (200), and (220) planes of the Pt crystal, respectively, and also produced a blue shift. In addition, a broad diffraction peak at $2\theta = 23^\circ$ appeared in both the Pt–AuNPs/CNFs and the PtNPs/CNFs, which is ascribed to the crystalline structure of the graphitic carbon [(120) plane] in the nanofibers. The above results further confirmed the fabrication of the Pt–AuNPs/CNFs.

Meanwhile, the XPS spectra of the Pt–AuNPs/CNFs, PtNPs/CNFs and AuNPs/CNFs are shown in Fig. 4. There are two clearly identifiable peaks for the Pt–AuNPs/CNFs in Fig. 4a, b. The Pt 4f peaks can be observed at 75.7 and 72.4 eV, which are associated with the binding energies of the Pt 4f_{5/2} and the Pt 4f_{7/2}, respectively, while the Au 4f peaks can be observed at 87.8 and 84.2 eV, which are associated with the binding energies of the Au 4f_{5/2} and the Au 4f_{7/2}, respectively. Compared with the corresponding Pt 4f peaks of the PtNPs/CNFs and the Au 4f peaks

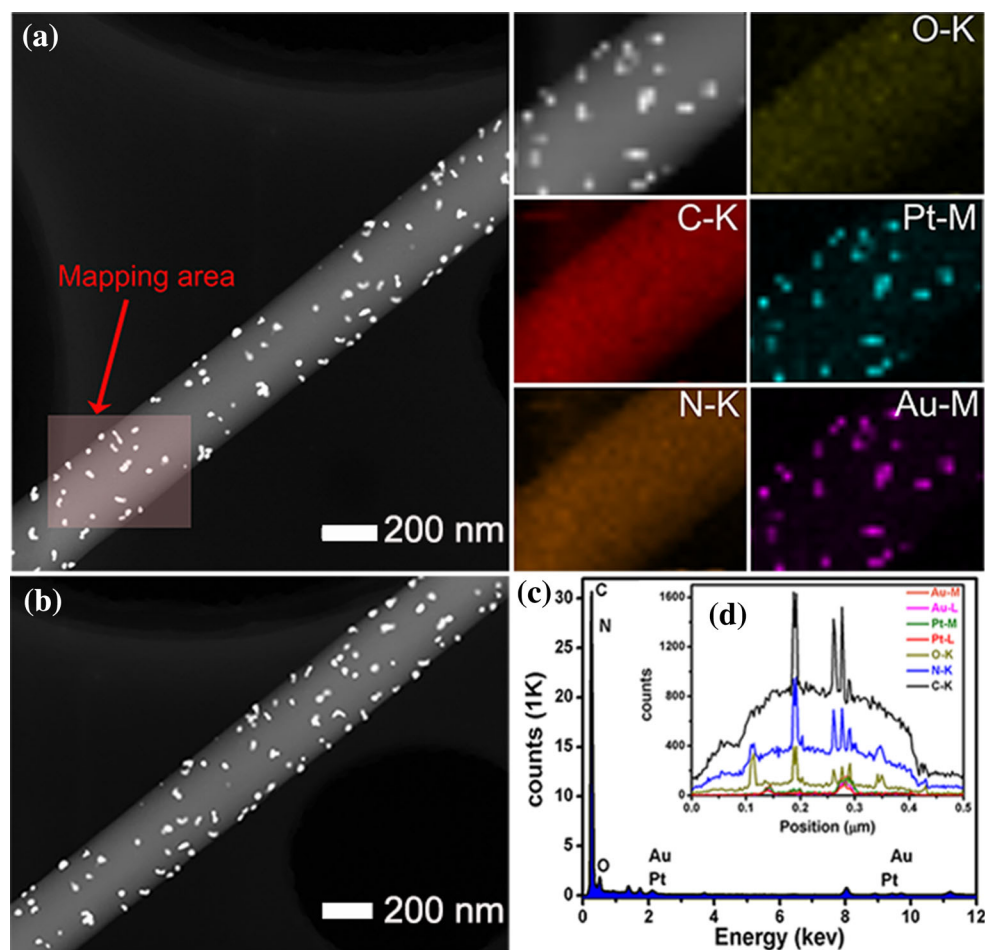


Figure 2 a The HAADF-STEM images of the Pt–AuNPs/CNFs, and STEM-EDS mapping images of the *selected area* indicated on the left. b The line-scanned area. c The EDX spectrum of the Pt–AuNPs/CNFs. d The line-scanned EDX spectrum for all of the elements.

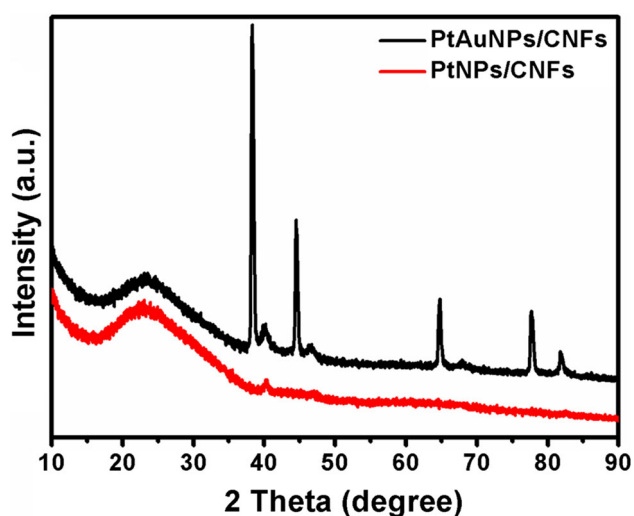


Figure 3 XRD patterns of the Pt–AuNPs/CNFs and the PtNPs/CNFs.

of the AuNPs/CNFs in Fig. 4c, d, there are a 0.3 eV red shift and a 0.2 eV blue shift for the Pt 4f peaks and the Au 4f peaks, respectively. Compared with PtNPs/CNFs, the Pt 4f XPS of Pt–AuNPs/CNFs demonstrates slight shift, which is ascribed to the change of Pt chemical environment and the electron transfer effect between Pt and Au, resulting in obviously changed B.E. of Pt–AuNPs/CNFs. All in all, the XPS results further indicating the formation of the Pt–AuNPs/CNFs. Therefore, the XPS results are consistent with the FE-SEM, STEM and XRD results.

Electroanalytic performance of the Pt–AuNPs/CNF-modified electrode (Pt–AuNPs/CNFs/GCE)

As an excellent electrode material, the electroanalytic performance of the Pt–AuNPs/CNFs as biosensors

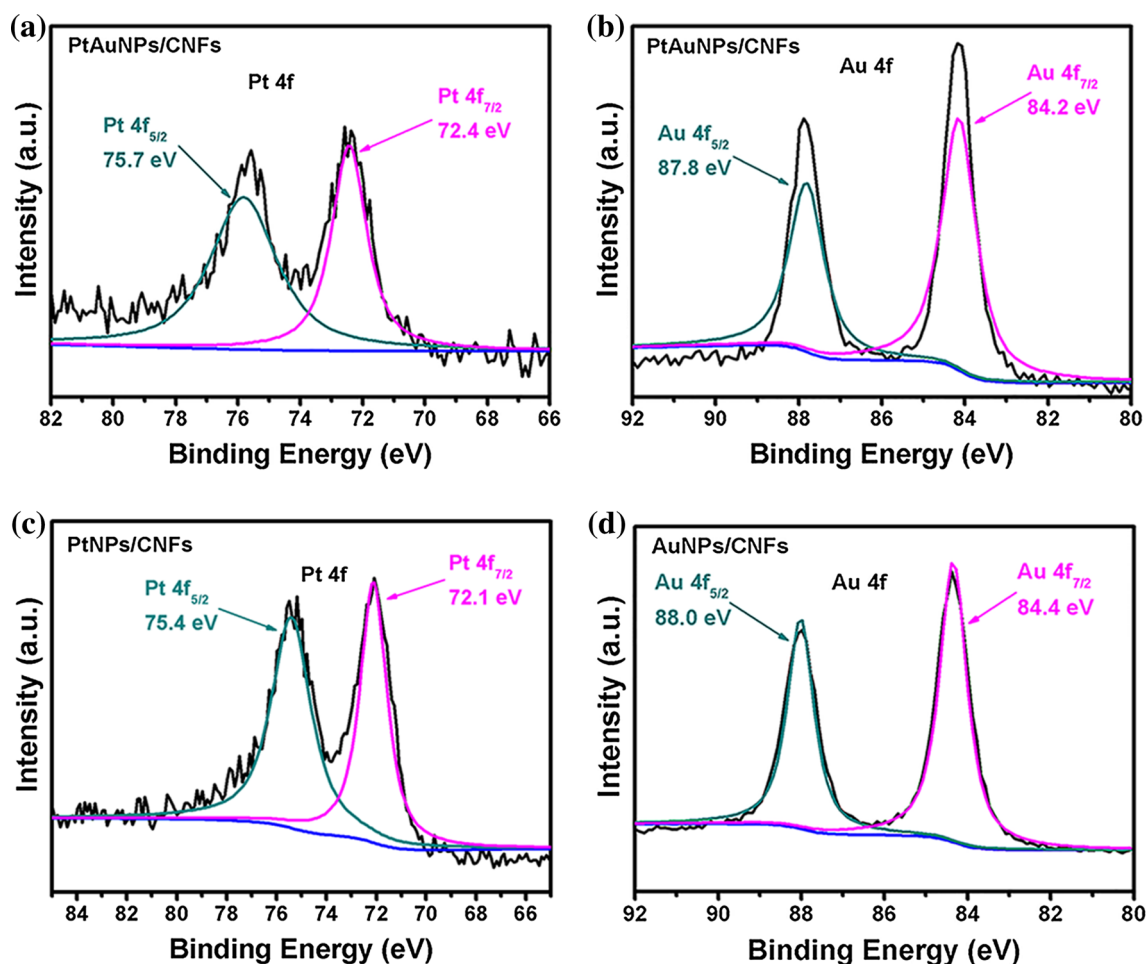


Figure 4 a–b XPS spectra of the Pt 4f and the Au 4f of the Pt–AuNPs/CNFs. c The XPS spectrum of the Pt 4f of the PtNPs/CNFs. d The XPS spectrum of the Au 4f of the AuNPs/CNFs.

was evident. Based on the well-dispersed Pt–AuNPs, we constructed a biosensor for the sensitive detection of H_2O_2 . To clarify the electrochemical activity of the Pt–AuNPs/CNFs/GCE, we performed an experiment on the electrode using a cyclic voltammogram (CV). The bare and modified electrodes were immersed in a neutral solution of 5 mM $\text{K}_3[\text{Fe}(\text{CN})_6]$, and the corresponding CV signals are shown in Fig. 5a, which are in the potential range from -0.6 to 1.2 V (vs. SCE) with a scan rate of 50 mV s^{-1} . The Pt–AuNPs/CNFs/GCE had a couple of well-defined oxidation and reduction peaks. Furthermore, the Pt–AuNPs/CNFs/GCE exhibited a significantly higher peak current and a larger peak area, indicating that the as-prepared Pt–AuNPs/CNFs possess excellent electrochemical activity and have potential for use in the field of H_2O_2 detection. Figure 5b shows the CV signals of the detection solutions in the absence and

presence of 5.0 mM of H_2O_2 using the modified Pt–AuNPs/CNFs/GCE. A clear signal obtained in the presence of H_2O_2 indicates the superior sensitivity of our Pt–AuNPs/CNFs. The response signals of the Pt–AuNPs/CNFs/GCE are shown in Fig. 5c. The signals correspond to the different scan rates ranging from 20 to 300 mV s^{-1} in the presence of 5 mM H_2O_2 and show a high response current of $116 \mu\text{A}$ without an enzyme. With the increase in the scan rate, the peak currents increased gradually, suggesting the extraordinary electrochemical behavior of the Pt–AuNPs/CNFs. In addition, the CV responses for H_2O_2 at a scan rate of 50 mV s^{-1} for 10 cycles are shown in Fig. 5d. The shape and the peak current all remain nearly the same. Considering the aforementioned results, the as-prepared Pt–AuNPs/CNFs exhibit good stability and electroanalytic performance for the detection of H_2O_2 .

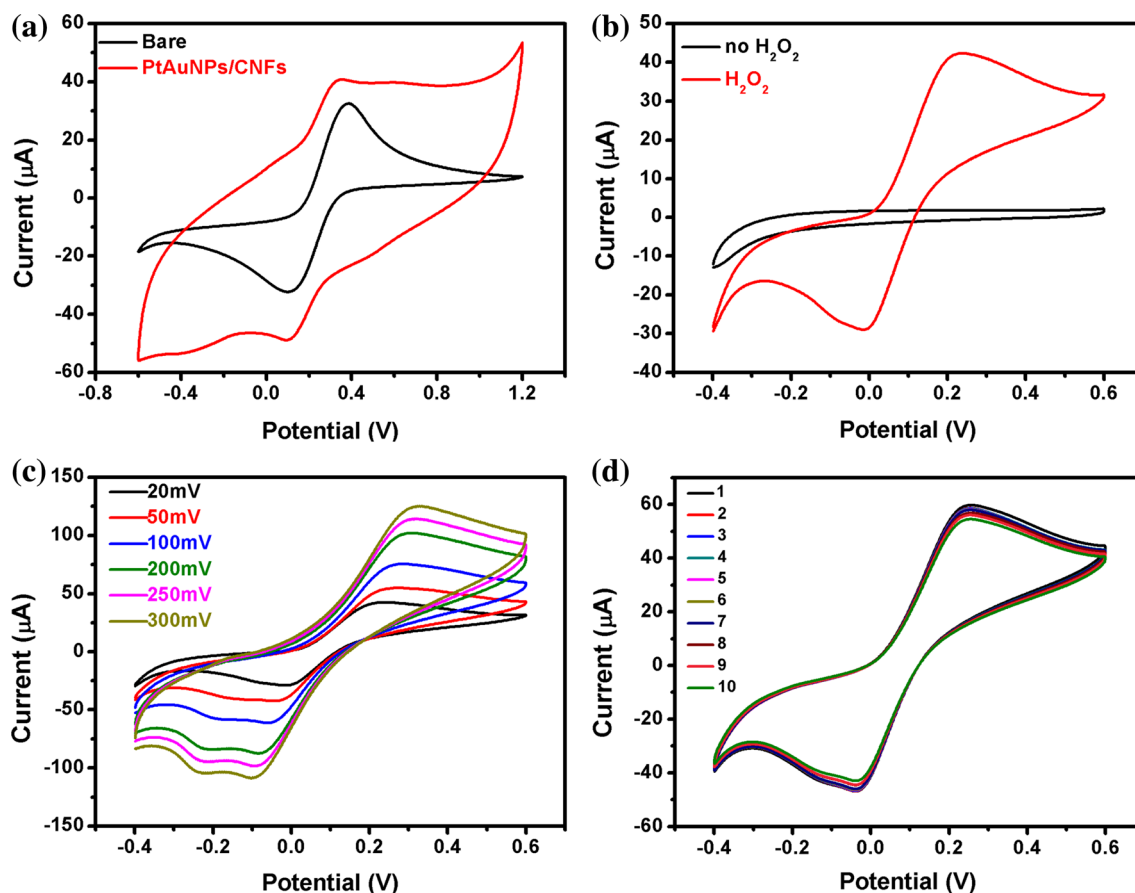


Figure 5 **a** CV responses of the bare GCE and the Pt–AuNPs/CNFs/GCE in a solution of 5 mM $K_3[Fe(CN)_6]$ with steps from -0.6 to 1.2 V versus SCE. The CV signals of the detection solutions **b** in the absence and presence of 5.0 mM of H_2O_2 and

c in the presence of 5 mM H_2O_2 at different scan rates from 20 to 300 $mV\ s^{-1}$. **d** The CV responses for H_2O_2 at a scan rate of 50 $mV\ s^{-1}$ for 10 cycles.

Electrocatalytic performance of the Pt–AuNPs/CNFs/GCE

As is well known, the hydrogen evolution reaction (HER) is an important indicative reaction for evaluating the electrocatalytic performance of an electrocatalyst. To characterize the electrocatalytic HER activity of the Pt–AuNPs/CNFs/GCE, we performed a series of electrochemical experiments in a 0.5 M H_2SO_4 solution with the modified GCE, as shown in Fig. 6. A commercial 20 wt% Pt/C electrocatalyst was used for comparison, and the PtNPs/CNFs and the AuNPs/CNF-modified electrode are also presented in Fig. 6a, b. It is easily seen that the AuNPs/CNFs have a relative high overpotential of 450 mV at 10 mA/cm^2 . Compared with the AuNPs/CNFs, the PtNPs/CNFs have a relatively lower overpotential of 380 mV at 10 mA/cm^2 . Interestingly, the designed Pt–AuNPs/CNFs with a low Pt content (3.09 wt%)

and Au content (5.89 wt%) exhibit the lowest overpotential of 235 mV at 10 mA/cm^2 , which is close to that of the Pt/C catalysts (45 mV), indicating optimal electrocatalytic HER activity.

Generally, the Tafel slope is key for characterizing HER activity. Catalysts with smaller Tafel slopes will better accelerate the HER rate, especially in practical applications [50–52]. As shown in Fig. 6b, the Tafel plots of the Pt–AuNPs/CNFs/GCE were obtained from the polarization curves. To ascertain the Tafel slopes, the black linear portions of polarization curves were fitted to the Tafel equation ($\eta = b \log j + a$, where j represents the current density, b represents the Tafel slope, and η represents the overpotential). The Tafel slopes of the AuNPs/CNFs and the PtNPs/CNFs are 130 and 108 $mV\ decade^{-1}$, respectively, indicating that both are probably involved in the Volmer reaction in the catalytic process. Meanwhile, the Pt–AuNPs/CNFs show a distinct

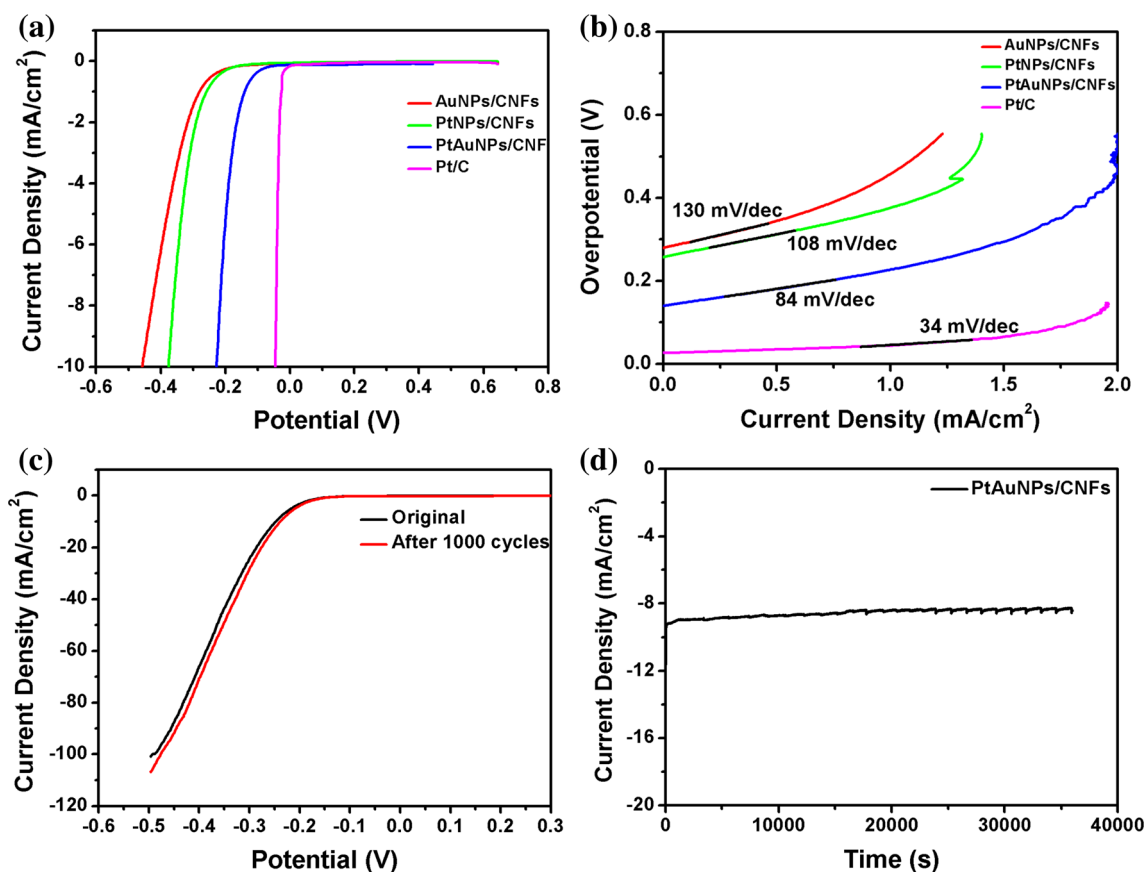


Figure 6 **a** Polarization curves (after iR-correction) of several of the as-prepared catalysts, as indicated, and **b** the corresponding Tafel plots. **c** The durability test of the Pt–AuNPs/CNFs/GCE.

d The current–time plot of the Pt–AuNPs/CNFs/GCE in 0.5 M H_2SO_4 at an applied potential of -0.25 V (vs. RHE).

improvement with a Tafel slope of $84 \text{ mV decade}^{-1}$, indicating that the main catalytic processes are the Volmer reaction and the Heyrovsky reaction. Notably, the Pt content of the as-prepared Pt–AuNPs is only 3.09%, and the content of Pt is smaller than that of the commercial Pt/C (20 wt%). The perfect HER activity is probably attributed to the homogeneous structure of the Pt–AuNPs, which combined the excellent catalytic activity of Pt with the excellent analytic ability of Au. In the present study, the as-prepared Pt–AuNPs/CNFs not only possess the high conductivity of CNFs but also exhibit the high surface-specific area of the exposed Pt–AuNPs, leading to excellent HER performance.

Furthermore, as an important assessment factor for the HER performance of a catalyst, the stability was studied in our research, as shown in Fig. 6c, d and it can be found that the Pt–AuNPs/CNFs/GCE exhibited good stability in HER. In detail, Fig. 6c shows that even after continuous cycling testing of 1000

cycles, the polarization curve of the Pt–AuNPs/CNFs/GCE remained nearly unchanged. To further confirm the favorable stability of the Pt–AuNPs/CNFs/GCE, the current–time plot is presented in Fig. 6d, which was performed under the condition of an applied potential of -0.32 V for the 12 h electrocatalysis measurement. There was almost no loss of electrocatalytic activity, even after continuing the test for such a long time at a certain potential. Based on the above discussion, we can draw the conclusion that the as-prepared Pt–AuNPs/CNFs possess good durability during the process of the extended electrochemical measurement. Furthermore, it is of great potential for practical application.

In summary, the size-controlled Pt–AuNPs/CNFs hybrid, synthesized via an electrospinning technique and an in situ thermal reduction method, exhibits good electrochemical activity, which can be attributed to the following reasons: (1) The specific nanostructure of the Pt–AuNPs/CNFs provides more

effective active sites for electrochemical behavior, which was beneficial for the adsorption capability and for the catalysis reaction of Pt–AuNPs/CNFs; (2) the well-dispersed and small-sized Pt–AuNPs exhibited a larger surface-specific area and are expected to enhance the electron transfer rate and improve the response signals; (3) CNFs possess either high electrical conductivity or excellent stability, contributing to the favorable electron transport capability and excellent durability of modified electrode; and (4) the bimetallic nanoparticles combined the excellent electroanalytic performance of Au with the superior electrocatalytic activity of Pt and demonstrated good bifunctional electrochemical properties that may have great potential application. In addition, in the fabrication process of the size-controlled Pt–AuNPs, no other reagents were used in the experiments. Therefore, the present study provided a facile and green method for the design and synthesis of noble metal NP/CNF materials. Moreover, the specific nanostructure of the as-prepared Pt–AuNPs/CNFs may have great potential in other electrochemical fields.

Conclusions

Pt–AuNPs/CNFs were successfully designed and fabricated via electrospinning technology and an in situ thermal reduction. The size-controlled Pt–AuNPs were evenly distributed on the surface of the CNFs. The Pt–AuNP/CNF-modified electrode with low Pt content was used as the working electrode for the electrochemical measurements. The novel nanostructure of the Pt–AuNPs combines the excellent electroanalytic performance of Au with the superior electrocatalytic activity of Pt and exhibits good electrochemical activity as a bifunctional catalyst for HER and the detection of H_2O_2 . The Pt–AuNP/CNF hybrid with low Pt content was utilized as a bifunctional electrocatalyst, exhibiting a higher response current of $116 \mu\text{A}$ without an enzyme for the detection of H_2O_2 and a lower overpotential ($j = 10 \text{ mA cm}^{-2}$ at -235 mV) and Tafel slope ($84 \text{ mV decade}^{-1}$) for HER compared to those of the PtNPs/CNFs and AuNPs/CNFs. This was ascribed to the specific nanostructure of the well-dispersed Pt–AuNPs, the favorable electron transport capability, the excellent durability of the CNFs, and the enhanced surface-specific area of the Pt–AuNPs/

CNFs. This study offers a green and facile method for constructing a specific bimetallic nanostructure for application in catalytic fields.

Acknowledgements

This study was supported by the National Natural Science Foundation of China (NSFC) (Grant No. 51373154, 51573166) and Science and Technology Planning Project of Zhejiang Province, China (Grant No. 2016F82G5420207).

References

- [1] Zhang J, Sasaki K, Sutter E, Adzic R (2007) Stabilization of platinum oxygen-reduction electrocatalysts using gold clusters. *Science* 315:220–222
- [2] Rice CR, Ha S, Masel RI (2003) Catalysts for direct formic acid fuel cells. *J Power Sources* 115:229–235
- [3] Zhang S, Shao YY, Yin GP, Lin YH (2010) Electrostatic self-assembly of a Pt-around-Au nanocomposite with high activity towards formic acid oxidation. *Angew Chem* 49:2211–2214
- [4] Chen XY (2011) Nanoplatfom-based molecular imaging. Wiley, New York
- [5] Rodríguez-fernández D, Liz-marzán LM (2013) Janus particles: metallic janus and patchy particles. *Part Part Syst Charact* 30:110
- [6] Liu XW, Wang DS, Li YD (2012) Synthesis and catalytic properties of bimetallic nanomaterials with various architectures. *Nano Today* 7:448–466
- [7] Mourdikoudis S, Chirea M, Zanaga D, Altantzis T, Mitrakas M, Bals S, Pastoriza-Santos I (2015) Governing the morphology of Pt–Au heteronanocrystals with improved electrocatalytic performance. *Nanoscale* 7:8739–8747
- [8] Yu Y, Sun Q, Liu X, Wu H, Zhou T, Shi G (2011) Size-controllable gold-platinum alloy nanoparticles on nine functionalized ionic-liquid surfaces and their application as electrocatalysts for hydrogen peroxide reduction. *Chemistry* 17:11314–11323
- [9] Duan SB, Wang RM (2013) Bimetallic nanostructures with magnetic and noble metals and their physicochemical applications. *Prog Nat Sci Mater Int* 23:113–126
- [10] Mao J, Chen Y, Pei J, Wang D, Li Y (2016) Pt–M (M = Cu, Fe, Zn, etc.) bimetallic nanomaterials with abundant surface defects and robust catalytic properties. *Chem Commun* 52:5985–5988
- [11] Zhu C, Wen D, Oschatz M, Holzschuh M, Liu W, Herrmann AK, Eychmüller A (2015) Kinetically controlled synthesis of

- PdNi bimetallic porous nanostructures with enhanced electrocatalytic activity. *Small* 11:1430–1434
- [12] Cao X, Wang N, Han Y, Gao C, Xu Y, Li M, Shao Y (2015) PtAg bimetallic nanowires: facile synthesis and their use as excellent electrocatalysts toward low-cost fuel cells. *Nano Energy* 12:105–114
- [13] Shen CC, Su J, Li X, Luo J, Yang M (2015) Electrochemical sensing platform based on Pd–Au bimetallic cluster for non-enzymatic detection of glucose. *Sens Actuators B Chem* 209:695–700
- [14] Xie RG, Chen MZ, Wang JQ (2015) Facile synthesis of Au–Pt bimetallic nanocomplexes for direct oxidation of methanol and formic acid. *RSC Adv* 5:650–653
- [15] Han C, Wu LE, Ge L, Li Y, Zhao Z (2015) AuPd bimetallic nanoparticles decorated graphitic carbon nitride for highly efficient reduction of water to H₂ under visible light irradiation. *Carbon* 92:31–40
- [16] Zhou Q, Lin Y, Lin Y, Wei Q, Chen G, Tang D (2016) Highly sensitive electrochemical sensing platform for lead ion based on synergetic catalysis of DNAzyme and Au–Pd porous bimetallic nanostructures. *Biosens Bioelectron* 78:236–243
- [17] Zhang J, Wan L, Liu L, Deng Y, Zhong C, Hu W (2016) PdPt bimetallic nanoparticles enabled by shape control with halide ions and their enhanced catalytic activities. *Nanoscale* 8:3962–3972
- [18] Mayrhofer K, Bliznac BB, Arenz M, Stamenkovic VR, Ross PN, Markovic NM (2005) The impact of geometric and surface electronic properties of Pt-catalysts on the particle size effect in electrocatalysis. *J Phys Chem B* 109:11444–14433
- [19] Tian N, Zhou Z, Sun SG, Ding Y, Wang ZL (2007) Synthesis of tetrahedral platinum nanocrystals with high-index facets and high electro-oxidation activity. *Science* 316:732–735
- [20] Li D, Meng F, Wang H, Jiang X, Zhu Y (2016) Nanoporous AuPt alloy with low Pt content: a remarkable electrocatalyst with enhanced activity towards formic acid electro-oxidation. *Electrochim Acta* 190:852–861
- [21] Lv J, Wang A, Ma X, Xiang RY, Chen JR, Feng JJ (2015) One-pot synthesis of porous Pt–Au nanodendrites supported on reduced graphene oxide nanosheets toward catalytic reduction of 4-nitrophenol. *J Mater Chem A* 3:290–296
- [22] Lee S, Jang H, Jang HY, Hong S, Moh SH, Park S (2016) Synthesis and optical property characterization of elongated AuPt and Pt@ Au metal nanoframes. *Nanoscale* 8:4491–4494
- [23] Félix-navarro RM, Beltrán-gastélum M, Reynoso-soto EA, Paraguay-Delgado F, Alonso-Nuñez G, Flores-Hernández JR (2016) Bimetallic Pt–Au nanoparticles supported on multi-wall carbon nanotubes as electrocatalysts for oxygen reduction. *Renew Energy* 87:31–41
- [24] Zhang S, Shao Y, Liao HG, Liu J, Aksay IA, Yin G, Lin Y (2011) Graphene decorated with PtAu alloy nanoparticles: facile synthesis and promising application for formic acid oxidation. *Chem Mater* 23:1079–1081
- [25] Takahashi S, Chiba H, Kato T, Endo S, Hayashi T, Todoroki N, Wadayama T (2015) Oxygen reduction reaction activity and structural stability of Pt–Au nanoparticles prepared by arc-plasma deposition. *Phys Chem Chem Phys* 17:11864–18638
- [26] Schrunner M, Proch S, Mei Y, Kempe R, Miyajima N, Ballauff M (2008) Stable bimetallic gold-platinum nanoparticles immobilized on spherical polyelectrolyte brushes: synthesis, characterization, and application for the oxidation of alcohols. *Adv Mater* 20:1928–1933
- [27] Luo J, Maye MM, Petkov V, Kariuki NN, Wang L, Njoki P, Zhong CJ (2005) Phase properties of carbon-supported gold-platinum nanoparticles with different bimetallic compositions. *Chem Mater* 17:3086–3091
- [28] Zhang S, Shao Y, Yin G, Lin Y (2010) Facile synthesis of PtAu alloy nanoparticles with high activity for formic acid oxidation. *J Power Sources* 195:1103–1106
- [29] Lu W, Ge J, Tao L, Cao X, Dong J, Qian W (2014) Large-scale synthesis of ultrathin Au–Pt nanowires assembled on thionine/graphene with high conductivity and sensitivity for electrochemical immunosensor. *Electrochim Acta* 130:335–343
- [30] Yoon J, Baik H, Lee S, Kwon SJ, Lee K (2014) One-pot synthesis of ultralong coaxial Au@ Pt nanocables with numerous highly catalytically active perpendicular twinning boundaries and Au@ Pt core-shell bead structures. *Nanoscale* 6:6434–6439
- [31] Liang YT, Lin SP, Liu CW, Chung SR, Chen TY, Wang JH, Wang KW (2015) The performance and stability of the oxygen reduction reaction on Pt–M (M = Pd, Ag and Au) nanorods: an experimental and computational study. *Chem Commun* 51:6605–6608
- [32] Xue M, Tan Y (2014) Hollow alloy nanostructures templated by Au nanorods: synthesis, mechanistic insights, and electrocatalytic activity. *Nanoscale* 6:11251–112500
- [33] Zhang M, Yan Z, Li Y, Jing J, Xie J (2015) Preparation of cobalt silicide on graphene as Pt electrocatalyst supports for highly efficient and stable methanol oxidation in acidic media. *Electrochim Acta* 161:48–54
- [34] Zhang LY, Zhao ZL, Li CM (2015) Formic acid-reduced ultrasmall Pd nanocrystals on graphene to provide superior electrocatalytic activity and stability toward formic acid oxidation. *Nano Energy* 11:71–77
- [35] Men B, Sun Y, Tang Y, Zhang L, Chen Y, Wan P, Pan J (2015) Highly dispersed Ag-functionalized graphene

- electrocatalyst for oxygen reduction reaction in energy-saving electrolysis of sodium carbonate. *Ind Eng Chem Res* 54:7415–7422
- [36] Chen S, Duan J, Tang Y, Jin B, Qiao SZ (2015) Molybdenum sulfide clusters-nitrogen-doped graphene hybrid hydrogel film as an efficient three-dimensional hydrogen evolution electrocatalyst. *Nano Energy* 11:11–18
- [37] Wang DY, Gong M, Chou HL, Pan CJ, Chen HA, Wu Y, Wang YL (2015) Highly active and stable hybrid catalyst of cobalt-doped FeS₂ nanosheets-carbon nanotubes for hydrogen evolution reaction. *J Am Chem Soc* 137:1587–1592
- [38] Ma C, Xu N, Qiao J, Jian S, Zhang J (2016) Facile synthesis of NiCo₂O₄ nanosphere-carbon nanotubes hybrid as an efficient bifunctional electrocatalyst for rechargeable Zn-air batteries. *Int J Hydrog Energy* 41:9211–9218
- [39] Chen S, Qi P, Chen J, Yuan Y (2015) Platinum nanoparticles supported on N-doped carbon nanotubes for the selective oxidation of glycerol to glyceric acid in a base-free aqueous solution. *RSC Adv* 5:31566–33157
- [40] Lee B, Park H, Cho MK, Jung JW, Kim HJ, Henkensmeier D, Jang JH (2016) Development of porous Pt/IrO₂/carbon paper electrocatalysts with enhanced mass transport as oxygen electrodes in unitized regenerative fuel cells. *Electrochem Commun* 64:14–17
- [41] Wang D, Zhou J, Hu Y, Yang J, Han N, Li Y, Sham TK (2015) In situ X-ray absorption near-edge structure study of advanced NiFe(OH)_x electrocatalyst on carbon paper for water oxidation. *J Phys Chem C* 119:11958–119573
- [42] Fu Y, Wang T, Su W, Yu Y, Hu J (2015) The electrocatalytic oxidation of carbohydrates at a nickel/carbon paper electrode fabricated by the filtered cathodic vacuum arc technique. *Electrochim Acta* 174:199–206
- [43] Yang Z, Kim C, Hirata S, Fujigaya T, Nakashima N (2015) Facile enhancement in co-tolerance of a polymer-coated Pt electrocatalyst supported on carbon black: comparison between Vulcan and Ketjenblack. *ACS Appl Mater Interfaces* 7:11589–115885
- [44] Higuchi E, Okada K, Chiku M, Inoue H (2015) Electrocatalytic activity for oxygen reduction reaction of Au core/Pt shell nanoparticle-loaded carbon black catalyst with different core sizes. *Electrochim Acta* 179:100–107
- [45] Qian H, Huang H, Wang X (2015) Design and synthesis of palladium/graphitic carbon nitride/carbon black hybrids as high-performance catalysts for formic acid and methanol electrooxidation. *J Power Sources* 275:734–741
- [46] Zou M, Du M, Zhu H, Xu C, Li N, Fu Y (2013) Synthesis of silver nanoparticles in electrospun polyacrylonitrile nanofibers using tea polyphenols as the reductant. *Polym Eng Sci* 53:1099–1108
- [47] Zhu H, Du ML, Zhang M, Zou M, Yang T, Wang L, Yao J, Guo B (2014) Probing the unexpected behavior of AuNPs migrating through nanofibers: a new strategy for the fabrication of carbon nanofiber–noble metal nanocrystal hybrids nanostructures. *J Mater Chem A* 2:11174–111728
- [48] Zhu H, Zhang M, Cai S, Cai Y, Wang P, Bao S, Du ML (2014) In situ growth of Rh nanoparticles with controlled sizes and dispersions on the cross-linked PVA–PEI nanofibers and their electrocatalytic properties towards H₂O₂. *RSC Adv* 4:794–804
- [49] Zhu H, Du ML, Zhang M, Wang P, Bao S, Zou ML, Yao JM (2014) Self-assembly of various Au nanocrystals on functionalized water-stable PVA/PEI nanofibers: a highly efficient surface-enhanced Raman scattering substrates with high density of “hot” spots. *Biosens Bioelectron* 54:91–101
- [50] Wang TY, Zhuo JQ, Du KZ, Chen BB, Zhu ZW, Shao YH, Li MX (2014) Electrochemically fabricated polypyrrole and MoS_x copolymer films as a highly active hydrogen evolution electrocatalyst. *Adv Mater* 26:3761–3766
- [51] Zhu H, Du ML, Zhang M, Zou ML, Yang TT, Wang SL, Yao JM, Guo BC (2014) S-rich single-layered MoS₂ nanoplates embedded in N doped carbon nanofibers: efficient co-electrocatalysts for hydrogen evolution reaction. *Chem Commun* 50:15435–15438
- [52] Zhao X, Zhu H, Yang XR (2014) Amorphous carbon supported MoS₂ nanosheets as effective catalysts for electrocatalytic hydrogen evolution. *Nanoscale* 6:10680–10685